Front. Struct. Civ. Eng. 2021, 15(3): 754–772
https://doi.org/10.1007/s11709-021-0711-2

RESEARCH ARTICLE

Effects of coarse and fine aggregates on long-term mechanical properties of sea sand recycled aggregate concrete

Jingwei YING[a,b], Yijie HUANG[a,b*], Xu GAO[a], Xibo QI[a], Yuedong SUN[a]

[a] *Shandong Key Laboratory of Civil Engineering Disaster Prevention and Mitigation, Shandong University of Science and Technology, Qingdao 266590, China*

[b] *Guangxi Key Laboratory of Disaster Prevention and Engineering Safety, Guangxi University, Nanning 530004, China*

[*] *Corresponding author. E-mail: 302huangyijie@163.com*

ABSTRACT Typical effects of coarse and fine aggregates on the long-term properties of sea sand recycled aggregate concrete (SSRAC) are analyzed by a series of axial compression tests. Two different types of fine (coarse) aggregates are considered: sea sand and river sand (natural and recycled coarse aggregates). Variations in SSRAC properties at different ages are investigated. A novel test system is developed via axial compression experiments and the digital image correlation method to obtain the deformation field and crack development of concrete. Supportive results show that the compressive strength of SSRAC increase with decreasing recycled coarse aggregate replacement percentage and increasing sea sand chloride ion content. The elastic modulus of SSRAC increases with age. However, the Poisson's ratio reduces after 2 years. Typical axial stress–strain curves of SSRAC vary with age. Generally, the effect of coarse aggregates on the axial deformation of SSRAC is clear; however, the deformation differences between coarse aggregate and cement mortar reduce by adopting sea sand. The aggregate type changes the crack characteristics and propagation of SSRAC. Finally, an analytical expression is suggested to construct the long-term stress–strain curve of SSRAC.

KEYWORDS sea sand recycled aggregate concrete, recycled coarse aggregate replacement percentage, sea sand chloride ion content, long-term mechanical properties, stress–strain curve

1 Introduction

The application of sea sand recycled aggregate concrete (SSRAC) is promising as it is a new type of environmentally friendly material. SSRAC enables natural coarse aggregates (NCAs) and fine aggregates to be replaced with demolished concrete and sea sand, respectively. SSRAC reduces the use of terrestrial resources (river sand, gravel, etc.), full utilizes ocean resources (sea sand), and decreases the output of construction waste. However, the typical mechanical properties of SSRAC are modified because of the coupled effects of recycled coarse aggregates (RCAs) and sea sand [1–4]. The use of SSRAC is restricted owing to the abovementioned reason. Further studies should be undertaken to promote its application.

Article history: Received Dec 30, 2019; Accepted Jun 22, 2020

Currently, investigations regarding SSRAC are few, and they pertain primarily to the analysis of the coupled effects of RCA and sea sand on the short-term mechanical properties of SSRAC [1]. Test results indicated that the sea sand chloride ion (Cl^-) content as well as RCA replacement percentage changed the properties of SSRAC significantly. The elastic modulus and strength increased with increasing sea sand Cl^- content and decreasing RCA replacement percentage. The typical effects of RCA on the strength of SSRAC were reduced by increasing sea sand Cl^- content [1]. Test results indicated that the compressive strength of 28 d SSRAC was higher than that of 28 d ordinary concrete (concrete adopting river sand and gravel) when the Cl^- content exceeded a certain value. Xiao et al. [3,5] and Zhang et al. [6] investigated the workability of seawater sea sand recycled aggregate concrete (SSSRAC) by performing a series of tests. It was shown that the fluidity

of SSSRAC was acceptable owing to the coupled effects of sea sand and RCA. The negative effect of RCA [5,7,8] on concrete workability reduced by adding sea sand [9,10]. Furthermore, the splitting strength of concrete using sea sand and RCA was on average 8% lower than that of ordinary concrete and 5% higher than that of recycled aggregate concrete (RAC). This is primarily because the coupled effects of Cl^- in sea sand (or seawater) and older mortar in RCA. The sea sand chloride ions slightly increased the SSRAC density and reduced its porosity [11–13], which decreased the negative effect of RCA on strength. The concrete absorption capacity reduced after sea sand was employed. This is because the effective volume of the liquid in concrete with sea sand increased. The macroscopic contact angle increased with the liquid effective volume when the triple contact line was pinned [14]. It was discovered that higher macroscopic contact angles resulted in inferior absorption capacity. The compressive strength of SSRAC developed rapidly at the early age; however, the development of strength decelerated after 28 d owing to Cl^- [1,4,15]. Limeira et al. [7] and Etxeberria et al. [11] observed that the negative effect of RCA on the water penetration maximum value of concrete reduced by adding Cl^-. The durability of SSRAC improved compared with that of RAC because of the coupled effects of Cl^- and RCA. Furthermore, Huang et al. [16] investigated the ductility and strength of confined SSRAC specimens. It was discovered that the basic mechanical properties of SSRAC enhanced by the outer tube confinement. Based on the research findings above, it can be concluded that the short-term properties of SSRAC was acceptable due to the coupled effects of sea sand and RCA.

However, current studies pertaining to the long-term mechanical properties of SSRAC are few. The coupled effects of sea sand and RCA on the properties of concrete at different ages were seldom investigated. Furthermore, current studies primarily focus on the macroscopic mechanical properties (strength, elastic modulus, ductility, etc.) and microstructure (interface transition zone, pore size, etc.) of SSRAC. The coupled effects of sea sand and RCA on the mechanical mechanism of specimens (deformation distribution and crack development) were seldom investigated. A novel test system was developed via axial compression experiments and the digital image correlation (DIC) method to investigate the macroscopic mechanical properties, deformation field, and crack development of SSRAC. Macro- and micro-level studies can be undertaken to analyze the effects of sea sand and RCA on the long-term properties of SSRAC. The research findings would provide a comprehensive insight into the elastic properties, plastic deformation, cracking and destroy of SSRAC.

2 Experimental section

2.1 Basic materials

For all concrete mixtures, 42.5R cement was adopted. Two types of coarse aggregates were considered: NCAs and RCAs. The size of coarse aggregates is 5–25 mm. The RCA was obtained from a demolished concrete pavement. Table 1 shows the typical properties of coarse aggregates [17]. It was discovered that the properties of the RCAs (crushing index, clay content, etc.) differed from those of the NCAs.

In this study, sea sand and river sand were adopted as the fine aggregates. Table 2 lists the properties of sea sand and river sand [18,19]. Three different sea sand chloride ion contents (0.050%, 0.081%, and 0.184%) were adopted in this study. It was discovered that the clay content of sea sand decreased compared with that of river sand.

2.2 Specimen preparation and design

2.2.1 Mix proportion

The actual mix proportion used was cement:water:coarse aggregates:fine aggregates = 320.3:205:1181.6:693.54. The water-to-cement ratio of specimen was 0.64. Additional water was considered because of the high water adsorption of the RCAs. The specific amount of additional water was obtained based on the RCA properties.

Table 1 Properties of coarse aggregate

material	bulk density (kg/m^3)	apparent density (kg/m^3)	water absorption	clay content	crushing index
NCA	1562	2580	0.9%	0.8%	7.6%
RCA	1416	2490	6.9%	8.6%	11.7%

Table 2 Properties of fine aggregates

material	clay content	apparent density (kg/m^3)	size (mm)	shell content	Cl^- content
sea sand	0.82%	2545	0.15–2.2	1.18%	0.050%/0.081%/0.184%
river sand	2.81%	2603	0.15–2.25	0%	0%

2.2.2 Preparation

All concrete mixtures were prepared based on the same procedures. 1) The cement and 1/3 of the mixing water were added, and the mixture was mixed for 2 min. 2) The aggregates and 1/3 of the water were used, and the concrete mixture was mixed for approximately 1 min. 3) The remaining water was used, and the concrete mixture was uniformly mixed. 4) Finally, the concrete mixture was filled into the mold. All specimens were cured under standard conditions (room temperature: 20°C±1°C; relative humidity: 90%±5%) until the test day (i.e., 7, 14, 28, and 100 d; 1 and 2 years).

2.2.3 Specimen design

Table 3 shows the details of the specimen. In the experiment, 12 sets of specimens were used. Two parameters were considered: RCA replacement percentage and sand Cl^- content. Each group comprised 24 prismatic concrete, 24 cubic concrete, and 3 sliced concrete (100 mm × 100 mm × 15 mm). The cubic and prismatic concrete were utilized to investigate the macroscopic mechanical properties (compressive strength and failure pattern, etc.). Additionally, the sliced concrete was obtained from the cubic concrete using a rock cutter, and it was adopted to analyze the deformation field and crack development of the SSRAC using the DIC method. Related findings from the DIC method can enable one to understand and quantify the changes in the macroscopic mechanical properties. Typical images of sliced SSRAC specimens are shown in Fig. 1.

All specimens are denoted by "SSRAC + RCA replacement percentage + sea sand Cl^- content" (Table 3). For example, "SSRAC-BC" represents SSRAC adopting 50% RCA replacement percentage (the first symbol "A", "B", and "C" represent 0%, 50%, and 100% RCA replacement percentages, respectively) and 0.081% sea sand Cl^- content (the second symbol "A", "B", "C", and "D" represent 0%, 0.05%, 0.081%, and 0.184% sea sand Cl^- contents, respectively).

2.3 Loading system and procedure

To analyze the long-term mechanical properties of SSRAC, two loading systems were used in this test.

2.3.1 Prismatic and cubic concrete

2.3.1.1 Loading system

The loading system included an electro hydraulic servo tester (2000 kN) and a computer (Fig. 2(a)). The actual compressive load and axial deformation were obtained using the computer.

2.3.1.2 Loading program

All specimens were preloaded with 10 kN prior to the actual test to reduce the negative effect of uneven loads and avoid the abnormal function of devices [1]. To ensure quasi-static loading, the displacement loading pattern was utilized (0.05 mm/min) [20]. The prismatic specimen deformation was measured using strain gauges and displacement transducers, which were set at the mid-span of the specimen (100 mm) to reduce the effect of the testing device.

2.3.2 Sliced specimen

2.3.2.1 Loading system

The loading system for the sliced concrete specimen can be classified into three sections, where each section comprises the following, separately: a 400 kN Measure Test Simulate

Table 3 Details of specimen

specimen	NCA ($kg \cdot m^{-3}$)	RCA ($kg \cdot m^{-3}$)	river sand ($kg \cdot m^{-3}$)	sea sand ($kg \cdot m^{-3}$)	sea sand Cl^- content (%)	dry density ($kg \cdot m^{-3}$)
SSRAC-AA	1181.6	0.0	693.6	0.0	0	2355
SSRAC-BA	590.8	590.8	693.6	0.0	0	2335
SSRAC-CA	0.0	1181.6	693.6	0.0	0	2323
SSRAC-AB	1181.6	0.0	0.0	693.6	0.050	2373
SSRAC-BB	590.8	590.8	0.0	693.6	0.050	2350
SSRAC-CB	0.0	1181.6	0.0	693.6	0.050	2320
SSRAC-AC	1181.6	0.0	0.0	693.6	0.081	2395
SSRAC-BC	590.8	590.8	0.0	693.6	0.081	2352
SSRAC-CC	0.0	1181.6	0.0	693.6	0.081	2316
SSRAC-AD	1181.6	0.0	0.0	693.6	0.184	2405
SSRAC-BD	590.8	590.8	0.0	693.6	0.184	2394
SSRAC-CD	0.0	1181.6	0.0	693.6	0.184	2365

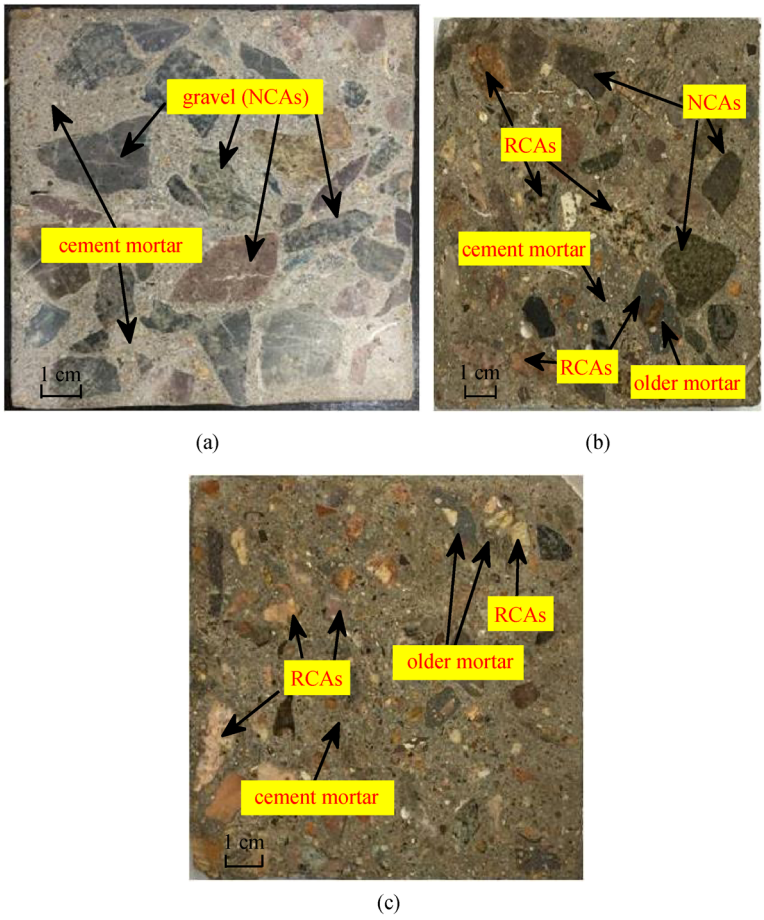

Fig. 1 Illustration of sliced concrete: (a) SSRAC-AA; (b) SSRAC-BA; (c) SSRAC-CA.

(MTS) tester, a black-and-white industrial camera (1 million resolution), and a workstation with an image analysis program (Fig. 2). The digital information of the specimen surface was obtained using the camera. The typical deformation field and the crack development were calculated using the image analysis program.

2.3.2.2 Loading program

A 2 kN load was applied to the sliced concrete prior to the actual testing to avoid the abnormal function of the loading system. The displacement mode was adopted as a loading pattern (0.07 mm/min). The axial deformation of sliced concrete was recorded using the displacement transducers and strain gauges. The data acquisition period was 0.5 s.

A video system (industrial camera) and a computer system were adopted to record the deformation development and crack distribution of the sliced concrete. The acquisition period of the image was 0.5 s. The typical failure process was obtained recorded using the camera.

3 Experimental results

3.1 Failure process

The axial-load–deformation relation of the SSRAC was linear at the beginning of the test. However, the load–deformation curve became nonlinear when the compressive load (F) reached 50%–70% of the peak value (F_{max}). A small crack appeared on the surface of the prismatic concrete when F approached 70%–90% of F_{max}. These fine cracks developed gradually and connected with each other at F_{max}. It was discovered that F decreased with increasing axial deformation after F_{max}. The transverse deformation of the specimen increased, and the width and length of the cracks increased rapidly. Finally, an inclined main macro-crack was formed, and the specimen failed.

The effect of the RCA on the failure of the SSRAC was clearer compared with that of sea sand. The test results indicated that the main cracks crossed the cement mortar and RCAs. However, the NCAs were rarely broken

(a) (b)

Fig. 2 Details of loading system: (a) prismatic and cubic concrete; (b) sliced concrete.

(Fig. 3). This is because the mechanical properties (stiffness and strength) of the RCAs were inferior to those of the NCAs. The effect of sea sand on the failure surface of the SSRAC was negligible. The typical failure surface of SSRAC-BA was similar to that of SSRAC-BD (Fig. 3).

The fine and coarse aggregates changed the failure angle (α) between the main cracks and axial direction. The α of SSRAC-AA (ordinary concrete) was 18°–35° but that of the SSRAC was 15°–25°. This is because the sea sand and RCA modified the concrete properties. Furthermore, the typical effect of age on the failure surface and failure angle was insignificant. The test results indicated that the failure pattern of SSRAC-BC at day 28 was similar to that of SSRAC-BC at 2 years.

3.2 Elastic modulus

3.2.1 Day 28

Table 4 shows the elastic modulus of specimen (E) at day 28. Generally, the value of E increased with an increase in sea sand Cl^- content and a decrease in RCA replacement percentage. However, the improvement in sea sand on E was reduced when the RCA replacement percentage was increased [1]. The test results indicated that E of SSRAC-AA at day 28 was approximately 6.8% and 0.7% higher than those of SSRAC-CA and SSRAC-CB, respectively. Compared with ordinary concrete (SSRAC-AA), the E of SSRAC increased when the sea sand Cl^- content exceeded 0.081%. This is because high Cl^- content significantly enhanced the microstructure of concrete and improved E [11,12]. However, the test results show that the E of SSRAC-BC was larger than those of SSRAC-AC and SSRAC-BD. This is attributable to the discreteness of concrete.

3.2.2 Development of E

The value of E increased with age (7, 14, 28, and 100 d; 1 and 2 years), irrespective of the types of fine and coarse aggregates. Furthermore, it was discovered that the development of E was affected by the RCAs and sea sand.

The higher the RCA content, the slower was the development of E. The test results indicated that the E of SSRAC-AA (ordinary concrete) at 7, 14, 28, and 100 d, as well as at 1 and 2 years was 12.9%, 9.0%, 7.3%, 25.6%, 27.0%, and 27.2% higher than that of SSRAC-CA at the same age (t), respectively. This is primarily caused by the excessive amount of older mortar and inferior interfacial transition zones (ITZs) in concrete adopting RCAs [21,22]. These impurities delayed the development of E.

Furthermore, the effect of Cl^- content on the development of E changed with age (Table 4). It was discovered that the E of specimens containing sea sand increased rapidly at the early age (before day 28) and developed slowly subsequently. Using SSRAC-AD and SSRAC-AA as examples, the E of SSRAC-AD at day 7, 14, 28, and 100, as well as 1 and 2 years was 16.3%, 19.9%, 14.7%, 4.65%, 3.98%, and 3.31% was higher than that of SSRAC-AA at the same age (t), respectively. This is because the sea sand Cl^- can accelerate the hydration of concrete at the early age (before day 28); however, the hydration of concrete may decelerate subsequently [3].

Finally, it can be concluded that the E of SSRAC developed slowly after day 28 compared with ordinary

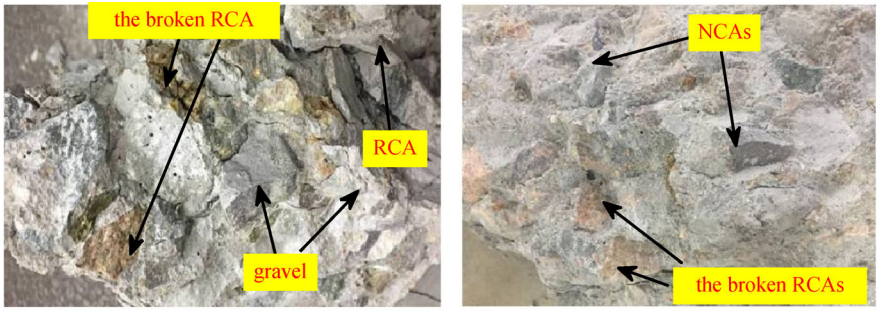

(a) (b)

Fig. 3 Failure surface of SSRAC: (a) SSRAC-BA; (b) SSRAC-BD.

Table 4 Elastic modulus and Poisson's ratio of SSRAC at different ages

specimen	E ($\times 10^4$ MPa)						υ	
	day 7	day 14	day 28	day 100	1 year	2 years	day 28	2 years
SSRAC-AA	1.992	2.001	2.147	2.657	2.745	2.808	0.246	0.241
SSRAC-BA	1.810	1.968	2.133	2.302	2.338	2.431	0.248	0.214
SSRAC-CA	1.764	1.836	2.001	2.115	2.160	2.209	0.255	0.192
SSRAC-AB	2.014	2.331	2.359	2.687	2.769	2.841	0.237	0.221
SSRAC-BB	1.967	1.961	2.212	2.341	2.387	2.462	0.231	0.209
SSRAC-CB	1.824	1.948	2.131	2.158	2.192	2.223	0.225	0.188
SSRAC-AC	2.047	2.369	2.450	2.619	2.720	2.869	0.210	0.213
SSRAC-BC	1.973	2.035	2.458	2.520	2.583	2.607	0.228	0.199
SSRAC-CC	1.872	1.962	2.214	2.225	2.238	2.261	0.203	0.186
SSRAC-AD	2.317	2.400	2.463	2.781	2.854	2.903	0.206	0.210
SSRAC-BD	2.034	2.178	2.289	2.367	2.404	2.452	0.198	0.193
SSRAC-CD	1.865	2.043	2.213	2.230	2.251	2.279	0.193	0.183

concrete. The E of SSRAC-AA at 2 years was 30.9% higher than that at day 28; however, the difference between the E of SSRAC-AA at 2 years and that of SSRAC-CD at day 28 was only 2.98%.

3.3 Poisson's ratio

3.3.1 Day 28

The Poisson's ratio (υ) increased with RCA content (Table 4). It was discovered that the υ of SSRAC-AA was approximately 0.81% and 3.66% lower than those of SSRAC-BA and SSRAC-CA, respectively. However, sea sand reduced the υ of SSRAC (day 28). This is because Cl^- improved the concrete microstructure and enhanced the modulus of SSRAC. Using SSRAC-AA as an example, the υ of SSRAC-AA was 3.71% and 14.7% higher than those of SSRAC-AB and SSRAC-AC, respectively.

Furthermore, improvements in the RCAs on υ reduced as the Cl^- content increased. The test results indicated that the υ of SSRAC-AC was 8.58% and −8.10% lower than those of SSRAC-BC and SSRAC-CD, respectively. Compared with ordinary concrete, the υ of SSRAC decreased under the coupled effects of RCA and sea sand.

3.3.2 Development of υ

It was discovered that υ decreased as the age of the aggregates progressed, irrespective of the aggregate type (i.e., fine or coarse) (Table 4). This occurred because the macro-and microstructures of concrete enhanced after long-term hydration. The deformability of SSRAC decreased as the aggregate age progressed. Compared with ordinary concrete (SSRAC-AA), the reduction in the υ of SSRAC was significant after 2 years. The υ of SSRAC-AA, SSRAC-BA, and SSRAC-CC at 2 years was 2.04%, 13.8%, and 8.38% lower than those of SSRAC-AA, SSRAC-CA, and SSRAC-CD at day 28, respectively. Furthermore, the υ of SSRAC decreased by 17% on average compared with that of ordinary concrete after 2 years.

3.4 Cubic compressive strength

3.4.1 Day 28

The SSRAC cubic compressive strength (f_{cu}) increased with an increase in Cl^- content and a decrease in RCA replacement percentage (Table 5). The positive effect of Cl^- content on f_{cu} was reduced by increasing the RCA replacement percentage. It was discovered that the f_{cu} of SSRAC-CA was approximately 6.18% lower than that of SSRAC-AA; however, the f_{cu} of SSRAC-CD was 3.65% higher than that of SSRAC-AA. This is attributable to the coupled effects of the fine and coarse aggregates. Numerous impurities, including inferior ITZs and older mortar in the RCAs, deteriorated the macro-and micro-structures of concrete [23]. Furthermore, it was discovered that the RCA decreased the density of SSRAC (Table 3). However, sea sand decreased the pore size and porosity of concrete and improved the microstructure of the specimen (Table 3) [7,11]. It was discovered that a higher sand Cl^- content resulted in a denser concrete microstructure and less effects by the RCA.

3.4.2 Development of f_{cu}

It was discovered that the value of f_{cu} increased as age (t) progressed. However, the sea sand and RCA changed the f_{cu} development.

The higher the RCA content, the slower was the development of f_{cu}. The test results showed that the f_{cu} of SSRAC-CA at day 7, 28, and 100, as well as 1 and 2 years was approximately 2.75%, 6.17%, 8.24%, 10.3%, and 10.6% lower than that of SSRAC-AA at the same age, respectively. However, the effect of sea sand on the development of f_{cu} changed as the specimen age progressed. The Cl^- accelerated the development of f_{cu} at the early age (before day 28). Furthermore, the f_{cu} of ordinary concrete (SSRAC-AA) at day 14 and 28 was 12.3% and 72.6% higher than that of SSRAC-AA at day 7, respectively. However, the f_{cu} of SSRAC-AD at day 14 and 28 was 26.9% and 98.4% higher than that of SSRAC-AD at day 7, respectively. Furthermore, the strength of SSRAC developed slowly after day 28 as the sea sand Cl^- content increased. The f_{cu} of SSRAC-AD at 2 years was 5.73% higher than that of SSRAC-AD at day 28, but the strength difference between SSRAC-AA at 2 years and day 28 was 7.2%. This is because Cl^- accelerated the concrete hydration at the early age but the hydration decelerated subsequently [3,5].

Compared with ordinary concrete (SSRAC-AA), the f_{cu} of SSRAC increased slowly. The sea sand and RCA changed the strength development of SSRAC.

3.5 Prismatic compressive strength

The day 28 prismatic compressive strength (f_c) of SSRAC decreased as the RCA content increased (Table 6). However, the negative effect of RCA on f_c was offset partially by sea sand. This is attributable to the change in the macro-and microstructures of SSRAC under the coupled effects of sea sand Cl^- and RCAs.

The effects of aggregates on the development of f_c were similar to those of aggregates on the development of f_{cu}. The RCAs delayed the increase in f_c. However, sea sand accelerated the increase in f_c at the early age and then decelerated the increase in strength after day 28. Compared with ordinary concrete, the effect of age on the f_c of SSRAC was negligible after 2 years.

The test results indicated that the ratio of f_c to f_{cu} (f_c/f_{cu}) increased as the age progressed, irrespective of the aggregate type. It was shown that the f_c/f_{cu} of SSRAC-CD at day 7, 28, and 100 as well as 2 years was 0.67, 0.68, 0.68, 0.81, 0.81, and 0.82, respectively. The f_c/f_{cu} of ordinary concrete (0.90) was similar to that of SSRAC (the average f_c/f_{cu} of SSRAC was 0.87) after 2 years.

Table 5 Cubic compressive strength of SSRAC at different ages (MPa)

specimen	day 7	day 14	day 28	day 100	1 year	2 years
SSRAC-AA	16.34	18.35	28.2	29.12	30.01	30.23
SSRAC-BA	15.01	20.11	27.9	28.14	29.03	29.75
SSRAC-CA	15.89	21.42	26.46	26.72	26.93	27.02
SSRAC-AB	17.16	23.98	29.65	30.78	31.55	30.71
SSRAC-BB	13.91	21.3	28.01	28.22	28.56	28.9
SSRAC-CB	13.93	17.78	26.36	24.51	25.92	27.31
SSRAC-AC	16.36	20.29	32.61	33.58	34.18	34.78
SSRAC-BC	16.56	20.25	28.11	27.43	29.21	30.42
SSRAC-CC	16.26	17.67	25.38	25.42	26.42	27.52
SSRAC-AD	17.06	21.66	33.84	34.66	35.22	35.78
SSRAC-BD	16.96	21.85	29.93	30.35	30.85	31.02
SSRAC-CD	16.47	21.09	29.23	29.69	30.17	30.59

Table 6 Prismatic compressive strength of SSRAC at different ages (MPa)

specimen	day 7	day 14	day 28	day 100	1 year	2 years
SSRAC-AA	11.41	14.44	18.59	25.95	26.88	27.15
SSRAC-BA	10.79	13.66	17.41	22.05	23.49	24.92
SSRAC-CA	9.71	13.08	15.90	21.89	22.65	23.13
SSRAC-AB	11.84	14.99	19.98	26.98	27.73	28.29
SSRAC-BB	11.06	15.63	19.87	26.74	26.43	26.59
SSRAC-CB	10.61	13.5	19.63	26.05	25.86	26.01
SSRAC-AC	12.09	16.56	21.40	26.65	28.3	29.67
SSRAC-BC	11.89	15.03	18.84	21.76	23.41	25.36
SSRAC-CC	10.82	13.95	17.72	20.07	22.83	24.44
SSRAC-AD	12.28	16.97	22.38	29.01	30.11	30.52
SSRAC-BD	12.02	15.53	19.86	25.03	25.36	25.51
SSRAC-CD	11.11	14.26	19.60	23.91	24.51	24.93

3.6 Axial stress–strain curve

The axial stress–strain curve (σ_c–ε_c curve) is typically used to describe the variation in the macroscopic mechanical properties of materials (plastic development and failure). A series of axial compression tests was performed to derive the σ_c–ε_c curve of SSRAC.

3.6.1 28-d curve

The typical σ_c–ε_c curves of SSRAC (28-d) are shown in Fig. 4. The curve comprised elastic, as well as elasto-plastic ascending and declining stages. At the elastic stage, the σ_c–ε_c curve was almost linear. The curve slope of SSRAC increased with increasing Cl^- content and decreasing RCA content. However, the σ_c–ε_c curve became nonlinear when the axial stress (σ_c) reached 40%–60% of the peak stress (f_c), owing to the developments of cracks and plastic deformation. Furthermore, the RCAs improved the curve curvature at this stage, whereas sea sand reduced the curve curvature (Fig. 4). The contributing factors are as follows. 1) The RCAs contained many ITZs and initial defects [19,24], which can accelerate the development of plastic deformation and microcracks. The higher the RCA content, the larger was the deformation and curve curvature. 2) The sea sand Cl^- decreased the porosity of SSRAC and increased its density, thereby improving the microstructure of SSRAC. A higher Cl^- content resulted in a smaller curve curvature.

Finally, the axial stress–strain curve exhibited a declining trend after f_c. It was observed that the RCAs and sea sand changed the decline of the curve slightly. The higher the RCA and Cl^- contents, the steeper was the decline of the curve. The concrete macroscopic mechanical properties were modified by adding RCAs and sea sand.

3.6.2 2-year curve

The 2-year stress–strain curves (σ_c–ε_c curves) of SSRAC are shown in Fig. 4. The curve comprised elastic, as well as elasto-plastic ascending and declining stages. As shown, the initial slope of the 2-year SSRAC curve was higher than that of the 28-d SSRAC curve (Figs. 4(a) and 4(b)). This is due to the degree of concrete hydration. A more complete concrete hydration resulted in a stiffer material and a higher initial curve slope. The typical effect of the RCAs on the curve slope was significant compared with that of sea sand Cl^- (Fig. 4(a)). That can be explained as follows: The sea sand Cl^- can accelerate the hydration of concrete at the early age (before day 28), but its effect on hydration becomes negligible subsequently. The curve slope of SSRAC containing high Cl^- content (SSRAC-BD) at 2 years was similar to that of the same specimen at day 28 (Fig. 4(b)).

When σ_c reached 40%–60% of f_c, the stress–strain curve was in the elasto-plastic ascending stage. It was shown that the RCAs increased the curve curvature, whereas sea sand Cl^- reduced the curve curvature (Fig. 4). The effect of Cl^- content on curve curvature was generally less than that of RCA replacement percentage (Fig. 4(b)). This is because Cl^- significantly improved the properties of SSRAC at the early age, whereas the effect became less prominent after day 28. Furthermore, f_c and the corresponding strain (ε_c) increased gradually with the age of the specimen. Compared with the effect of the RCAs, that of sea sand on f_c enhancement became insignificant after 2 years (Fig. 4).

The σ_c decreased with increasing ε_c after the peak point. The decline in the σ_c–ε_c curve became steeper after 2 years, irrespective of the aggregate type. However, a higher Cl^- content resulted in a less prominent effect of the specimen age. The decline in the SSRAC-AD curve was similar to

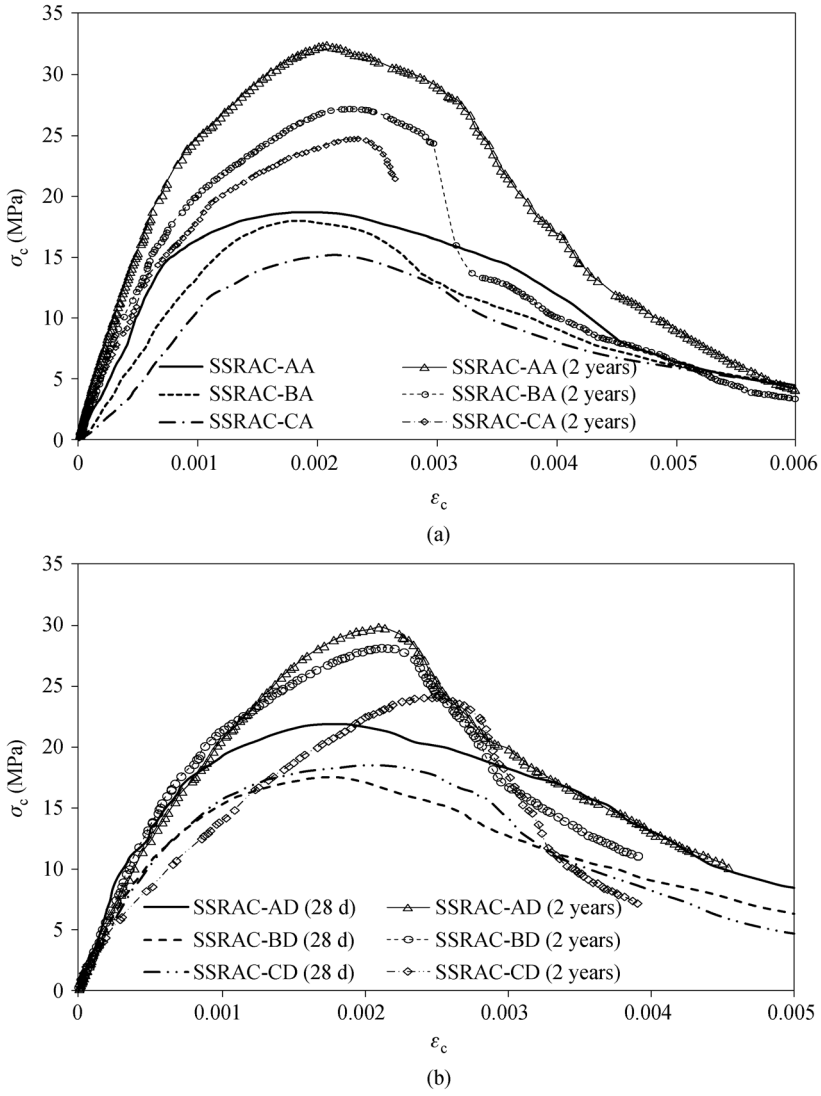

Fig. 4 Development of axial stress–strain curve at different ages: (a) RCA replacement percentage; (b) sea sand Cl^- content.

that of the SSRAC-BD curve (Fig. 4). This is attributable to the degree of concrete hydration. Increasing the sea sand Cl^- content can reduce the effect of age on the long-term properties of SSRAC. The macroscopic properties of concrete changed according to the RCA replacement percentage, Cl^- content, and age.

4 DIC analysis and discussion

A uniaxial compression experiment was performed on sliced SSRAC. The mechanical mechanism (deformation distribution and crack development) of SSRAC was investigated using the DIC method. The typical effects of fine and coarse aggregates on the long-term mechanical mechanism of SSRAC at macro- and microlevels were investigated. The results obtained using the DIC method can be used to validate the changes in the macroscopic mechanical properties of SSRAC. Details regarding the DIC numerical program are available in Refs. [25,26]. The MATLAB software was used to code the procedure involved. It was discovered that the DIC results were consistent with the test results. The average value and standard deviation of errors were 0.106 and 0.049 pixels, respectively.

4.1 Axial displacement distribution

Figure 5 shows the images of these test specimens. Typical axial displacement distribution contour maps of SSRAC-AA, SSRAC-BA, SSRAC-CA, and SSRAC-CD (2 years) under axial compression are shown in Figs. 6–7. The typical characteristics of axial displacement distribution at different stages were obtained as follows.

The axial displacement distribution of SSRAC changed significantly after different coarse aggregates instead of

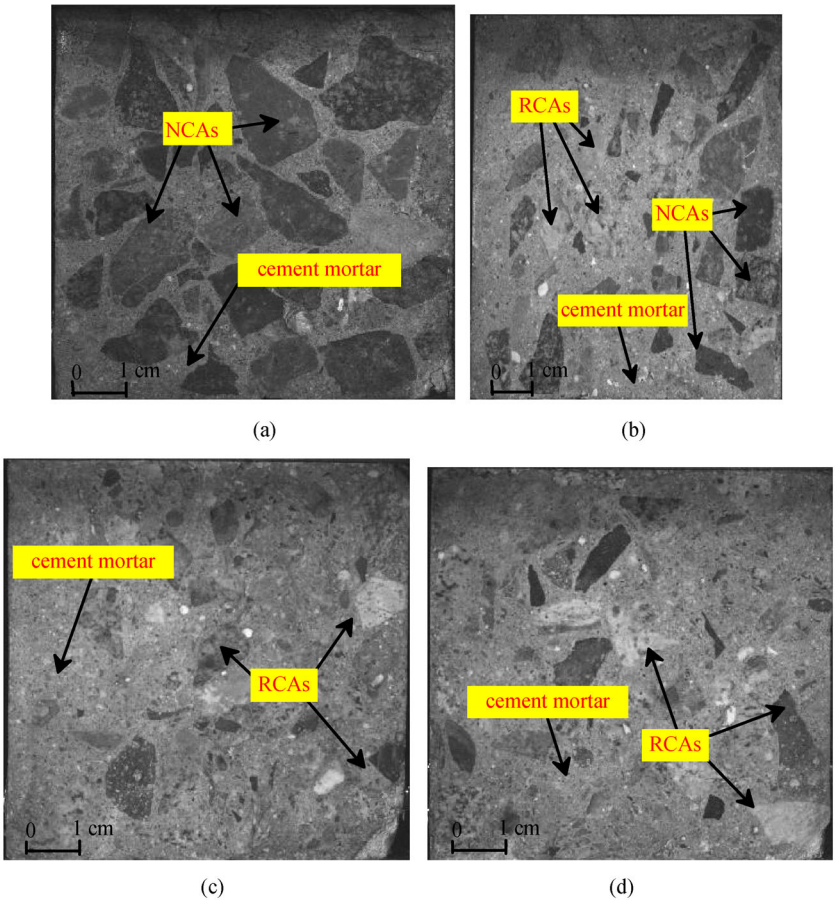

Fig. 5 Sliced specimen: (a) SSRAC-AA; (b) SSRAC-BA; (c) SSRAC-CA; (d) SSRAC-CD.

fine aggregates were used. At the early stage of the test (30% of the peak stress (σ_{max})), the NCA (gravel) axial displacement was lower than the cement mortar axial displacement (Figs. 6(a)–6(b)). This is attributable to the hardness of gravel being higher than that of cement mortar. The NCAs formed a strong skeleton and supported the external load. However, the RCA axial displacement was similar to the cement mortar axial displacement (Figs. 6(b)–6(c)). This is because the properties of the RCAs (modulus and hardness) were similar to those of cement mortar. The effect of coarse aggregates on axial displacement distribution decreased as the load increased. The test results indicated that the cement mortar axial displacement was similar to the NCA and RCA axial displacements (Figs. 7(a)–7(c)) when σ approached σ_{max} (macrocracks appeared in the specimen). This occurred because the contribution from the NCA skeleton reduced gradually when macrocracks appeared. After σ_{max}, the change in the deformation distribution of SSRAC and the effect of coarse aggregates became negligible.

Furthermore, the SSRAC axial displacement distribution was slightly altered when different fine aggregates were adopted. Using SSRAC-CD (SSRAC containing high sea sand Cl^- content (0.184%)) as an example, the cement mortar axial displacement was smaller than the RCA axial displacement in the initial stage of the test (Figs. 6(d)). This is because the Cl^- in sea sand decreased the pore size and porosity of concrete and improved the microstructure of the specimen. In the initial stage of testing (loading), a higher Cl^- content resulted in a denser microstructure of the cement mortar and less mortar displacement. However, the sea sand impact on the axial displacement distribution became negligible at σ_{max} (Fig. 7(d)). The deformation distribution of SSRAC changed when macrocracks appeared.

4.2 Strain distribution

4.2.1 Axial strain distribution

Figures 8–9 show the effects of coarse and fine aggregates on the axial strain distribution of the specimen at different stages. It was discovered that the high-value axial strain of SSRAC-AA (ordinary concrete) was primarily concentrated in the ITZs between the mortar and NCAs (Fig. 8(a)) when the axial stress (σ) approached 30% of the peak stress (σ_{max}). However, the high-value axial strain of SSRAC-CA (recycled concrete) was concentrated in both the ITZs and

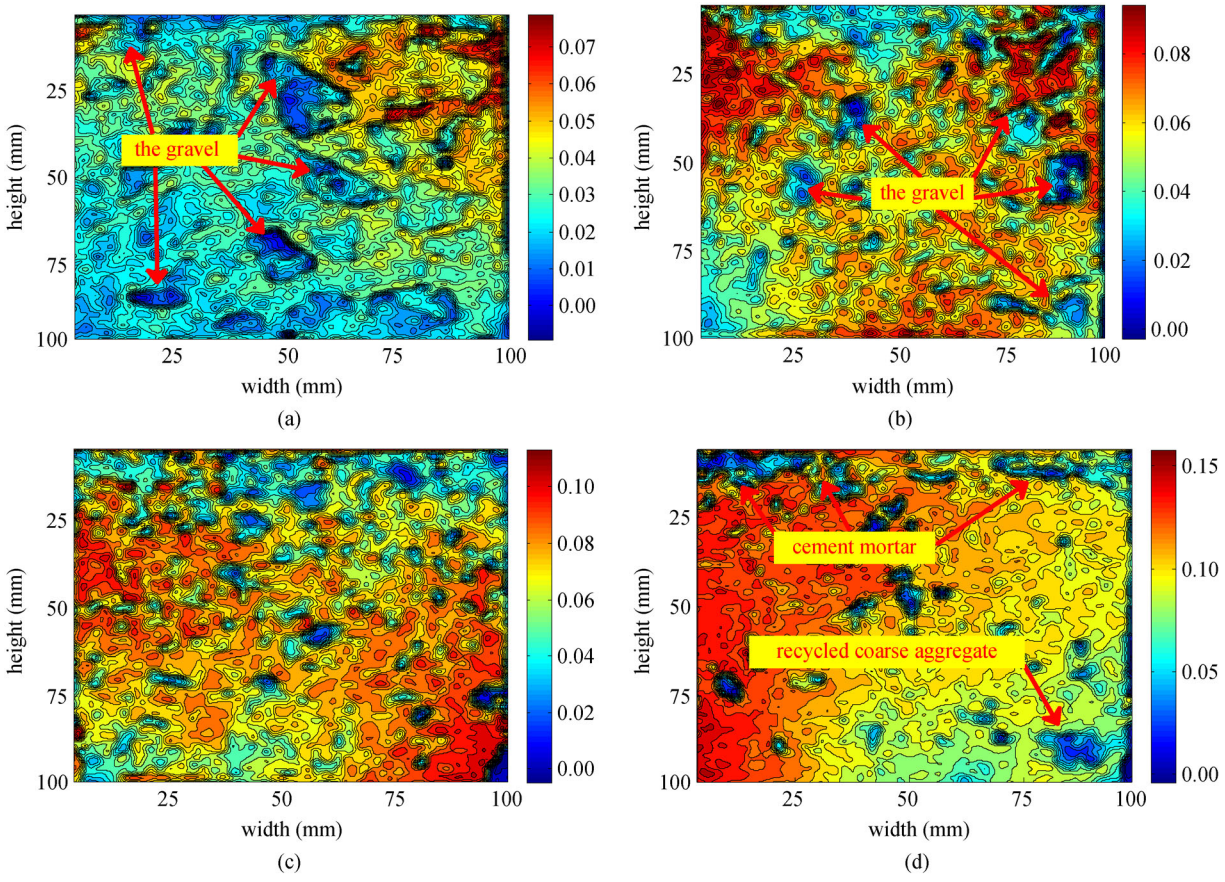

Fig. 6 SSRAC axial displacement at $0.3\sigma_{max}$ (units: mm): (a) SSRAC-AA; (b) SSRAC-BA; (c) SSRAC-CA; (d) SSRAC-CD.

cement mortar (Fig. 8(b)). This is due to differences in the properties of concrete components (mortar, gravel, RCA, etc.). The effect of the coarse aggregates on the axial strain distribution was slight at σ_{max}. However, compared with the high-value axial strain of SSRAC-AA, that of SSRAC-CA appeared in the RCAs when σ approached σ_{max} (Figs. 9(a)–9(b)).

Furthermore, the sea sand Cl^- imposed only a slight effect on the axial strain distribution. The SSRAC-CD strain distribution was similar to the SSRAC-CA strain distribution. However, compared with SSRAC-CA, more high-value strains appeared in the RCAs of SSRAC-CD at the early stage of the test (Figs. 8(b)–8(c)). This is because Cl^- improved the microstructure of cement mortar, resulting in similar properties between cement mortar and the RCAs. Furthermore, the test results show that the high-value axial strain of SSRAC-CD was inferior to that of SSRAC-CA when σ approached σ_{max}. This is caused by changes in the microstructure of cement mortar (Figs. 9(b)–9(c)).

4.2.2 Transverse strain distribution

The transverse strain distribution of the specimens is shown in Figs. 10–11. As shown, the transverse strain distribution was not uniform at the early stage of testing ($0.3\ \sigma_{max}$). The effects of the coarse and fine aggregates on the transverse strain distribution were negligible owing to the inhomogeneous concrete components.

The distribution of the high-value transverse strain changed with the age of the specimens. The high-value transverse strain of SSRAC-AA (ordinary concrete) at 2 years crossed those of gravel, mortar, and ITZs when σ approached σ_{max} (Fig. 11(a)). However, the high-value transverse strain of ordinary concrete at day 28 rarely appeared in gravel [16,18]. This is because the values of the properties of cement mortar (strength, modulus, etc.) increased significantly after 2 years.

Furthermore, the high-value transverse strain distribution of SSRAC-CA (recycled concrete) was similar to that of SSRAC-CD. The high-value transverse strain primarily appeared in cement mortar and the RCAs (Figs. 11(b)–11(c)). However, the amount of the high-value transverse strain increased with decreasing sea sand Cl^- content. Using SSRAC-CD as an example, the properties of cement mortar were similar to those of the RCAs under the coupled effects of age and Cl^- content, and they decreased the amount of the high-value transverse strain.

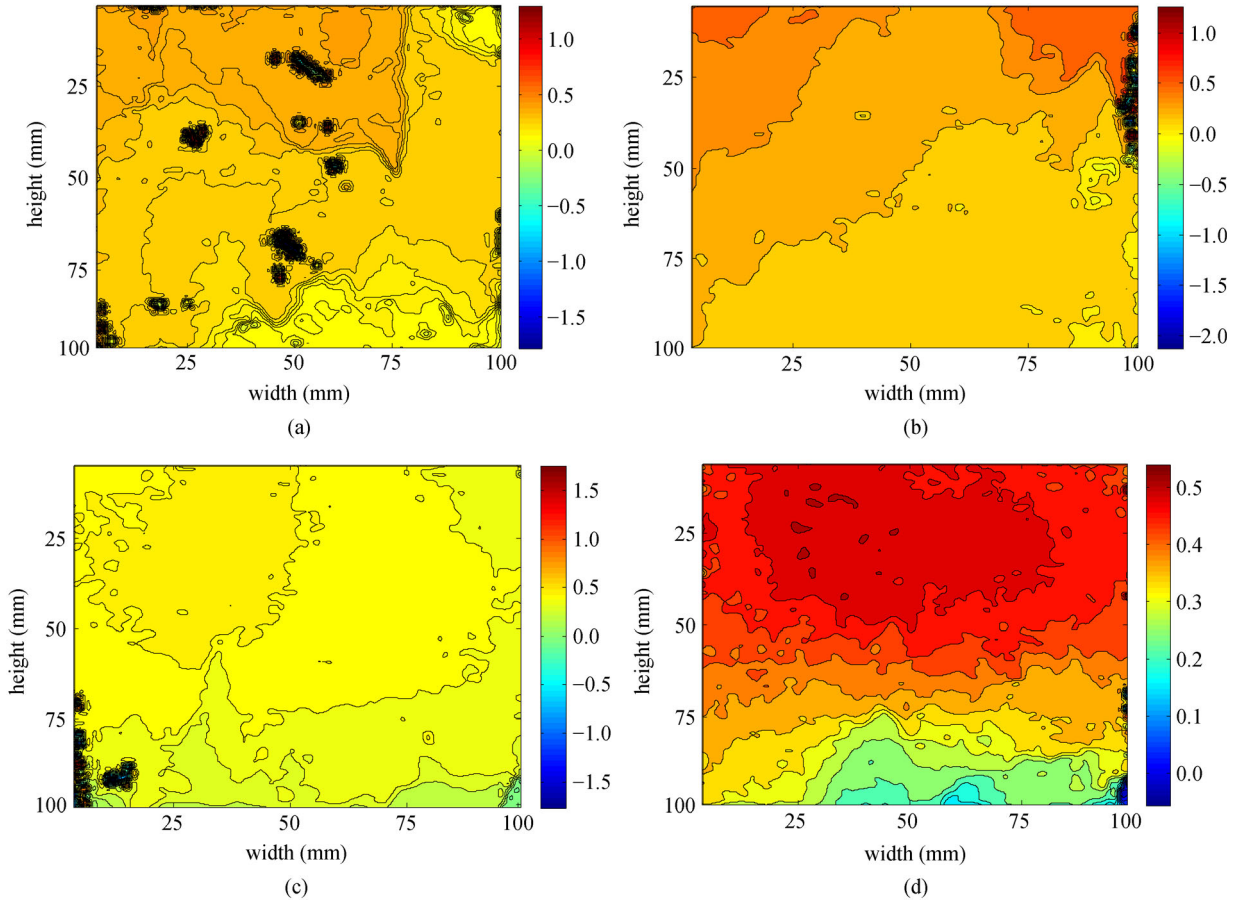

Fig. 7 SSRAC axial displacement at σ_{max} (units: mm). (a) SSRAC-AA; (b) SSRAC-BA; (c) SSRAC-CA; (d) SSRAC-CD.

4.3 Propagation of cracks

Figures 12–14 show the growth of cracks at different test stages. The crack characteristics changed with the variation in the coarse aggregate type. It was observed that the microcracks of SSRAC-AA first appeared in the ITZs (Figs. 12(a)–12(b)) at the early stage of the test ($0.5\sigma_{max}$). However, the microcracks of SSRAC-CA and SSRAC-CD appeared in cement mortar (Figs. 13(a)–13(b)). That is because the discrepancies between the gravel and cement mortar properties remained high after 2 years (ordinary concrete). The microcracks developed rapidly when σ approached $0.9\sigma_{max}$ (Figs. 12(c)–12(d)). It was shown that the cracks of SSRAC-AA primarily crossed the ITZs and cement mortar, and these macrocracks appeared in gravel after the peak point (Figs. 12(e)–12(f)). However, the macrocracks of SSRAC-CA and SSRAC-CD were concentrated in the RCAs and cement mortar at $0.9\sigma_{max}$ (Figs. 13(c)–13(d) and 14(c)–14(d)). It was discovered that the effect of the coarse aggregates on SSRAC crack propagation was significant even after 2 years.

Furthermore, the typical effect of sea sand on the crack characteristics was less compared with that of the coarse aggregates. The crack propagation of SSRAC-CD was similar to that of SSRAC-CA (Figs. 13–14). However, sea sand slightly changed the size of the cracks. It was observed that the amount and size of SSRAC-CD cracks were lower than those of SSRAC-CA when the axial stress approached σ_{max} (Figs. 13(c)–13(d) and 14(c)–14(d)). This occurred because Cl^- decreased the pore size and enhanced the microstructures of cement mortar. A denser mortar microstructure resulted in more similar properties between mortar and the RCAs and smaller cracks. However, the cracks of SSRAC-CD developed rapidly after the peak point (σ_{max}). Compared with the size and number of cracks of SSRAC-CA, those of SSRAC-CD were high when the axial stress reduced to $0.9\sigma_{max}$ (Figs. 13(e)–13(f) and 14(e)–14(f)). This is attributable to the fewer cracks and less plastic deformation in SSRAC-CD prior to σ_{max}.

5 Approximation of stress–strain relations

The aggregate type affected the long-term mechanical properties of concrete. However, analytical formulas for the long-term load–deformation relationship of SSRAC are few. Based on the experimental data and relevant results [1,16,19], a new expression that can describe the changes

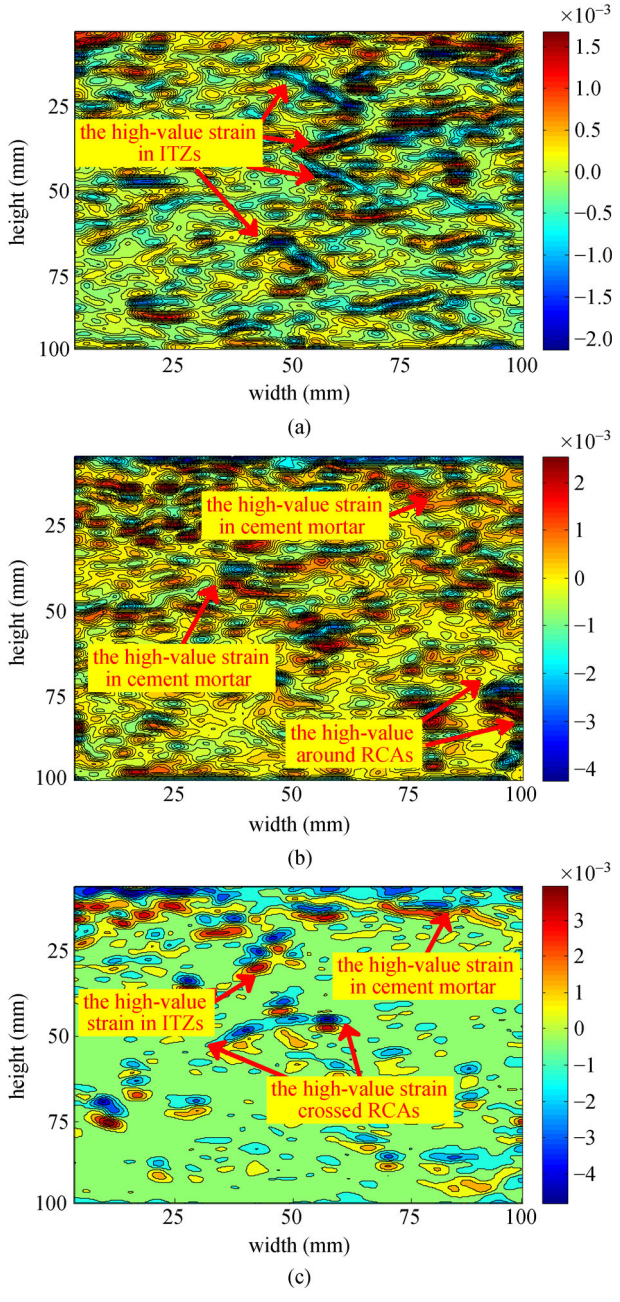

Fig. 8 SSRAC axial strain at $0.3\sigma_{max}$ (units: ε): (a) SSRAC-AA; (b) SSRAC-CA; (c) SSRAC-CD.

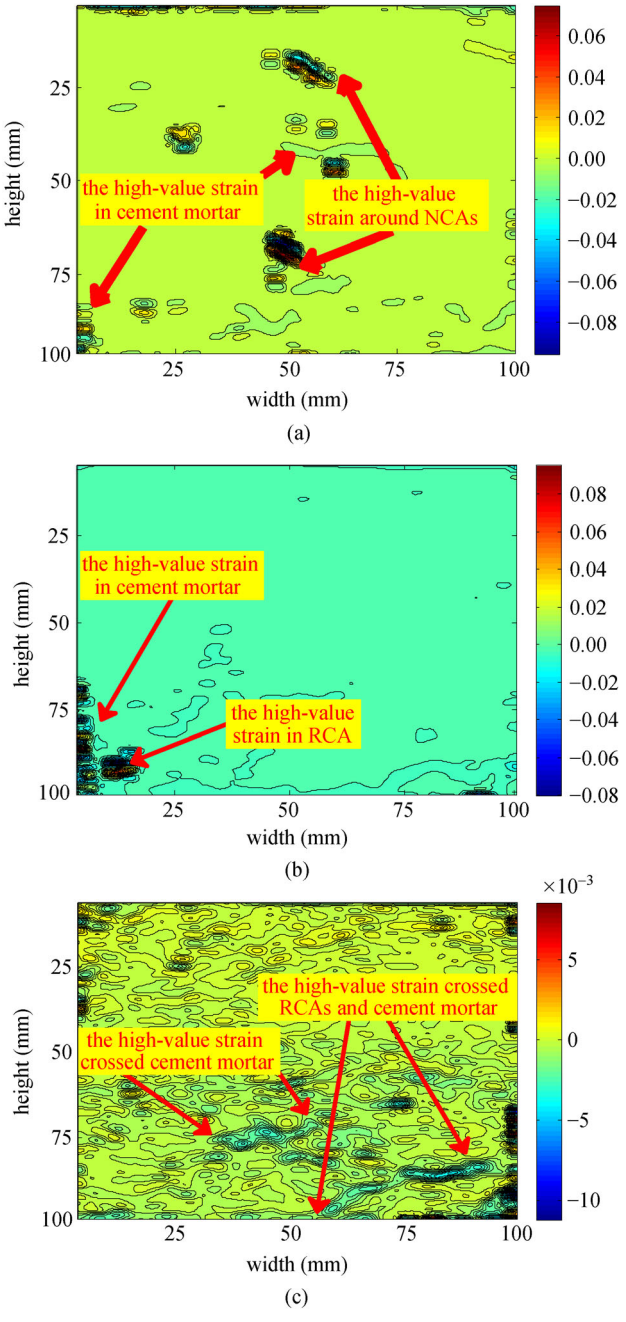

Fig. 9 SSRAC axial strain at σ_{max} (units: ε): (a) SSRAC-AA; (b) SSRAC-CA; (c) SSRAC-CD.

in the long term macroscopic mechanical properties of SSRAC (2 years) is proposed. The specific analytical stress–strain formula is shown in Eq. (1).

$$\eta = \begin{cases} a\omega + (3-2a)\omega^2 + (a-2)\omega^3, & 0 \leqslant \omega \leqslant 1, \\ \dfrac{\omega}{b(\omega-1)^2 + \omega}, & \omega > 1, \end{cases} \tag{1}$$

where $\eta = \sigma_c/f_c$, $\omega = \varepsilon_c/\varepsilon_o$, and ε_o is the peak strain of concrete. σ_c is the axial stress, and ε_c is the axial strain. a and b are calculated as follows.

5.1 a

The parameter a is the curve initial slope. A higher a implies a larger curvature of the curve.

$$a = 1.213[(0.552 - 7.94 \times 10^5\psi^2)r^2 - (0.637 - 963.73\psi)r + 45\psi + 2.29]. \tag{2}$$

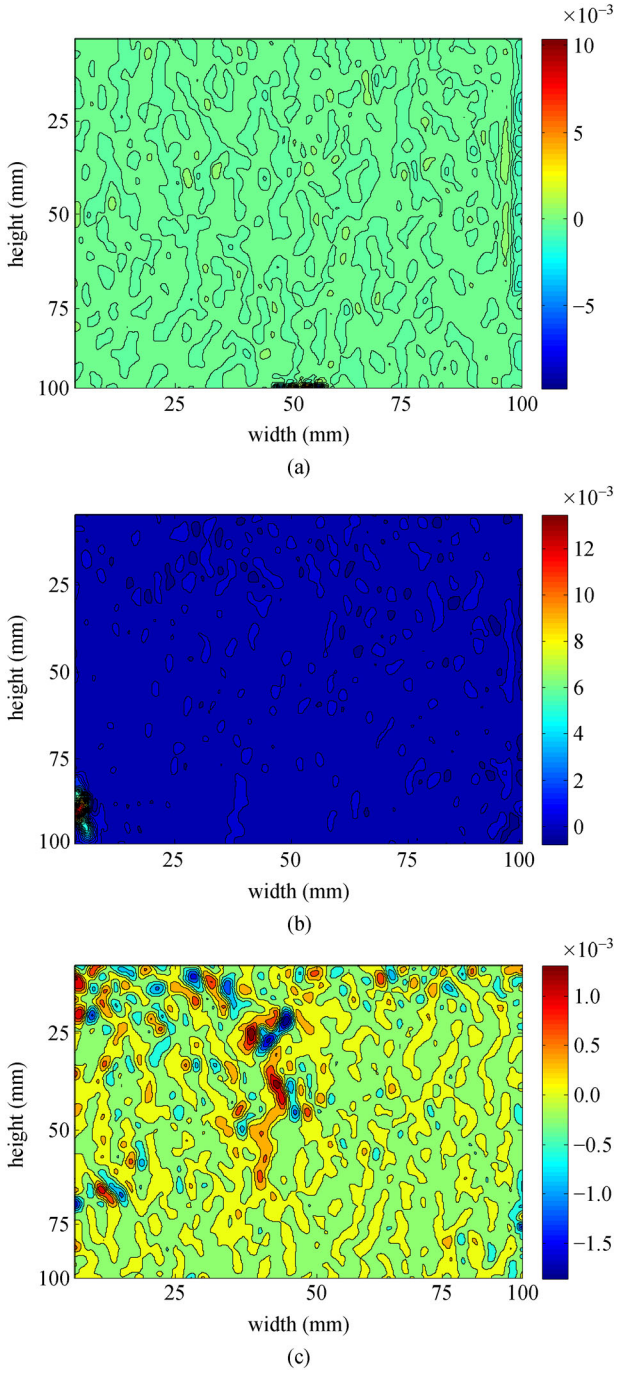

Fig. 10 SSRAC transverse strain at $0.3\sigma_{max}$ (units: ε): (a) SSRAC-AA; (b) SSRAC-CA; (c) SSRAC-CD.

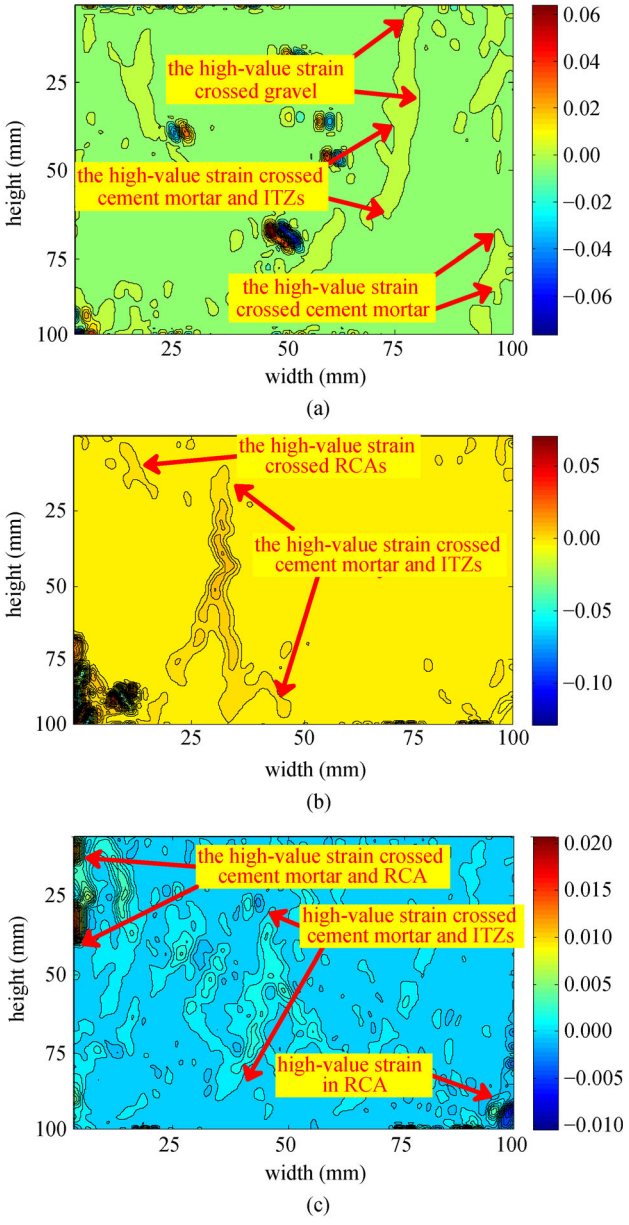

Fig. 11 SSRAC transverse strain at σ_{max} (units: ε). (a) SSRAC-AA; (b) SSRAC-CA; (c) SSRAC-CD.

In Eq. (2), ψ represents the Cl^- content, and γ represents the RCA replacement percentage.

5.2 *b*

The parameter b denotes the area under the declining part of curve (Eq. (3)). Generally, the ductility of a material decreases as b increases.

$$b = 2.51[(2.455 - 1264.255\psi)r + 198.136\psi + 1.121]. \quad (3)$$

Figure 15 shows the differences between the calculated and real curves. The test results indicated that the discrepancies were negligible. Therefore, the proposed analytical formulas can be adopted to design the SSRAC structure.

6 Conclusions

The long-term mechanical properties of SSRAC were

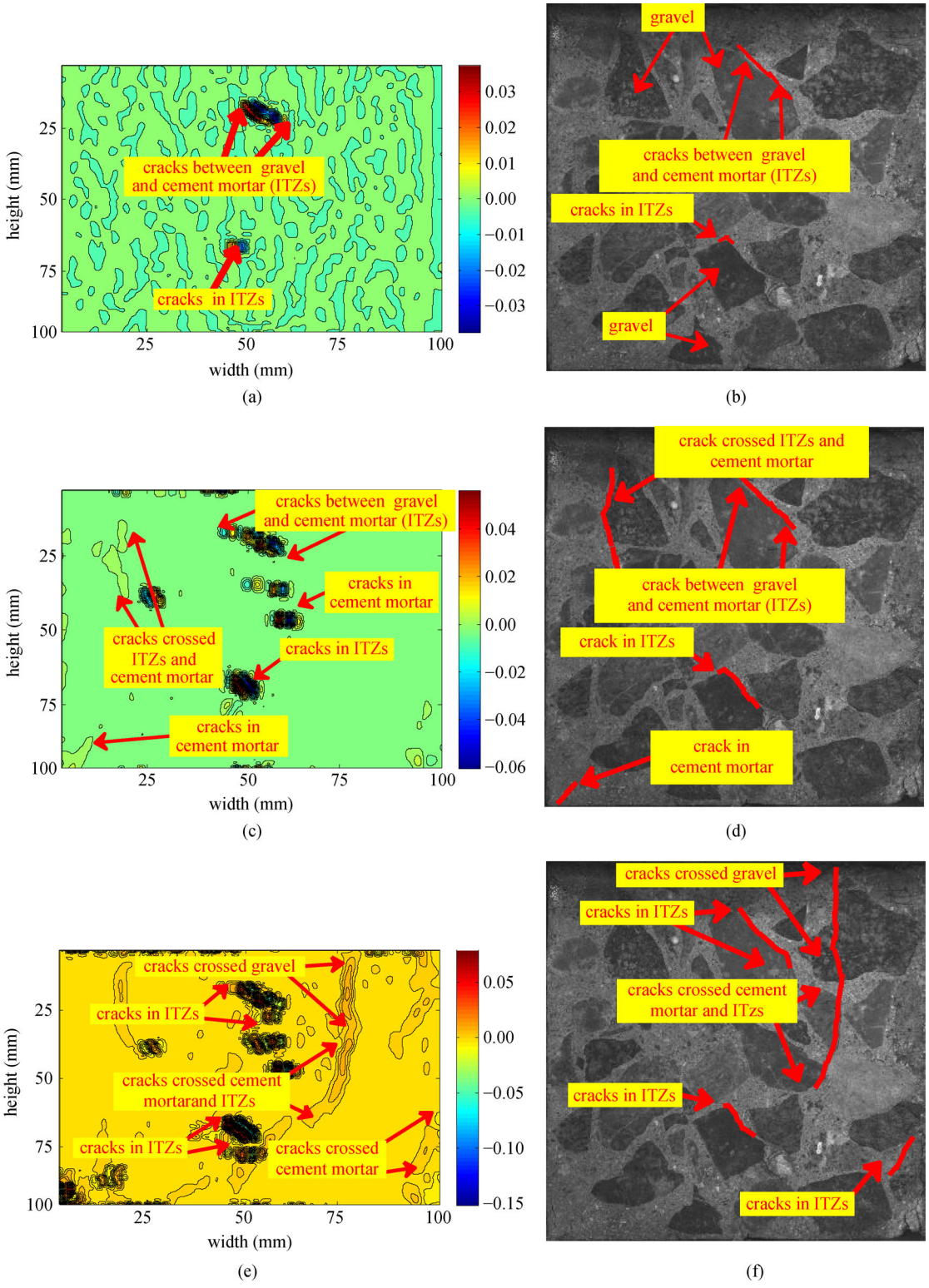

Fig. 12 SSRAC-AA crack propagation at different stages. (a) Transverse strain at $0.5\sigma_{max}$ shown in specimen (b); (c) transverse strain at $0.9\sigma_{max}$ shown in specimen (d); (e) transverse strain at $0.9\sigma_{max}$ (post peak point) shown in specimen (f).

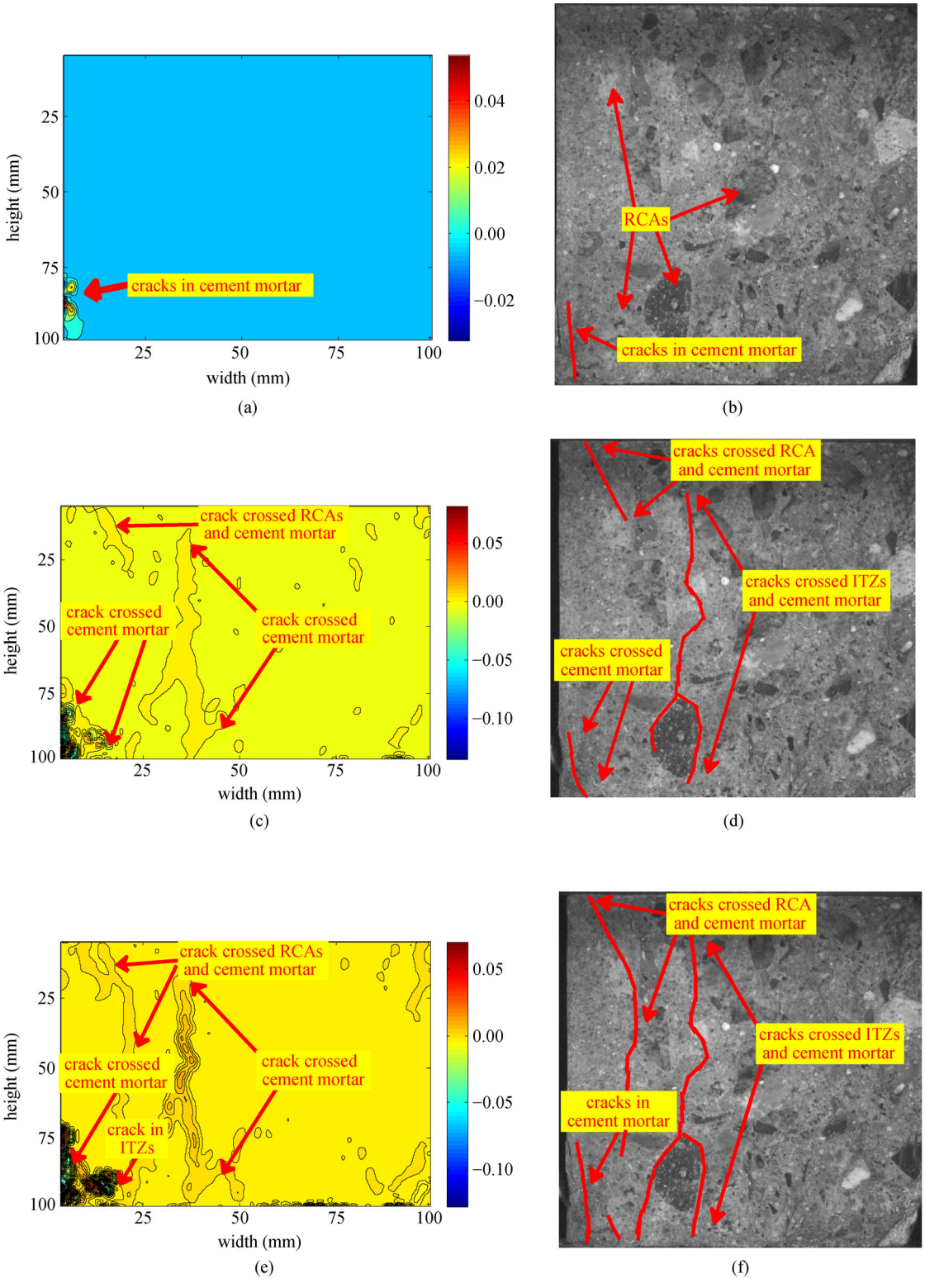

Fig. 13 SSRAC-CA crack propagation at different stages. (a) Transverse strain at $0.5\sigma_{max}$ show in specimen (b); (c) transverse strain at $0.9\sigma_{max}$ shown in specimen (d); (e) transverse strain at $0.9\sigma_{max}$ (post peak point) shown in specimen (f).

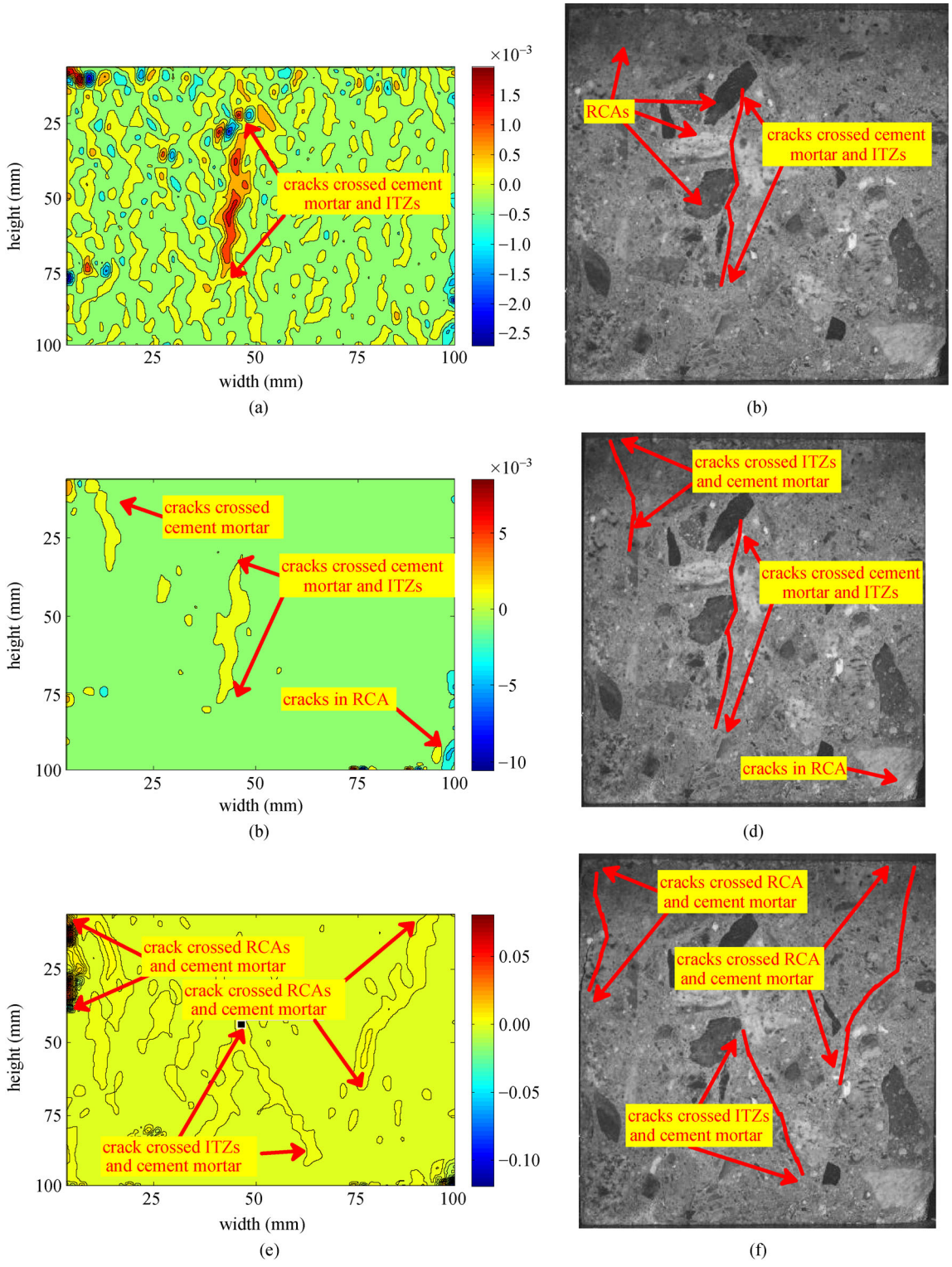

Fig. 14 SSRAC-CD crack propagation at different stages. (a) Transverse strain at $0.5\sigma_{max}$ shown in specimen (b); (c) transverse strain at $0.9\sigma_{max}$ shown in specimen (d); (e) transverse strain at $0.9\sigma_{max}$ (post peak point) shown in specimen (f).

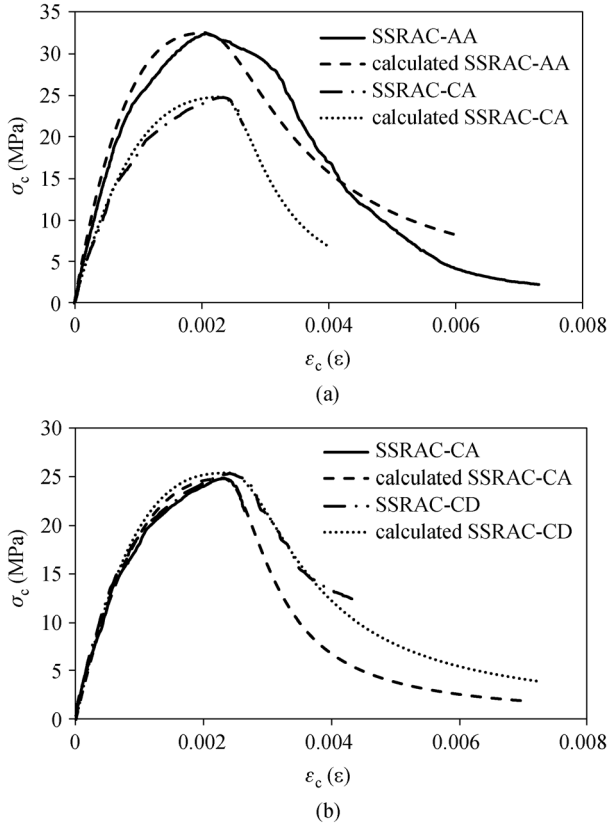

Fig. 15 Calculated stress–strain curves: (a) RCA replacement percentage; (b) sea sand Cl^- content.

tested and analyzed. The findings obtained are as follows.

1) The difference between the failure patterns of SSRAC and ordinary concrete was negligible. The effects of age and sea sand on the failure surface were insignificant compared with the effect of RCAs. The aggregate type affected the failure angle of SSRAC.

2) Increasing the RCA replacement percentage reduced the effect of sea sand Cl^- on the SSRAC elastic modulus. A higher RCA content resulted in a slower development of f_{cu}. Sea sand accelerated the development of f_{cu} at the early age. Furthermore, υ increased and f_c/f_{cu} decreased as the specimen age progressed, irrespective of the aggregate type (i.e., fine or coarse).

3) Sea sand decreased the curvature of the stress–strain curve, whereas the RCAs increased the curve curvature. The higher the RCA and Cl^- contents, the steeper was the curve decline. The initial slope of the curve increased, whereas the curve curvature decreased after 2 years. The effect of age on the stress–strain curve reduced when the sea sand Cl^- content was increased. A specific expression for the SSRAC stress–strain relationship considering the effects of age as well as fine and coarse aggregates was provided.

4) The effect of RCAs on the axial deformation distribution was more significantly compared with that of sea sand. However, changes in the SSRAC deformation distribution under different sea sand Cl^- contents and RCA replacement percentages decreased after the peak stress.

5) Higher RCA and sea sand Cl^- contents resulted in the earlier appearance of cracks in the coarse aggregates. The development of the high-value transverse strain changed after 2 years. Compared with the effect of the coarse aggregates, that of the fine aggregates on the characteristics of cracks was less.

Acknowledgements The authors would like to acknowledge the support provided by the National Natural Science Foundation of China (Grant Nos. 51408346, 51978389), the Systematic Project of Guangxi Key Laboratory of Disaster Prevention and Structural Safety (No. 2019ZDK035), and the Opening Foundation of the Shandong Key Laboratory of Civil Engineering Disaster Prevention and Mitigation (No. CDPM2019KF12).

References

1. Huang Y J, He X J, Wang Q, Sun Y D. Mechanical properties of sea sand recycled aggregate concrete under axial compression. Construction & Building Materials, 2018, 175: 55–63
2. Limeira J, Agullo L, Etxeberria M. Dredged marine sand as a new source for construction materials. Materiales de Construcción, 2012, 62(305): 7–24
3. Xiao J Z, Qiang C B, Nanni A, Zhang K J. Use of sea-sand and seawater in concrete construction: Current status and future opportunities. Construction & Building Materials, 2017, 155: 1101–1111
4. Li W G, Luo Z Y, Sun Z H, Hu Y, Duan W H. Numerical modelling of plastic-damage response and crack propagation in RAC under uniaxial loading. Magazine of Concrete Research, 2018, 70(9): 459–472
5. Xiao J Z, Zhang P, Zhang Q T, Shen J, Li Y, Zhou Y. Basic Mechanical properties of seawater sea-sand recycled concrete. Journal of Architecture and Civil Engineering, 2018, 35(2): 16–22 (in Chinese)
6. Zhang Q T, Xiao J Z, Liao Q X, Duan Z H. Structural behavior of seawater sea-sand concrete shear wall reinforced with GFRP bars. Engineering Structures, 2019, 189: 458–470
7. Limeira J, Etxeberria M, Agullo L, Molina D. Mechanical and durability properties of concrete made with dredged marine sand. Construction & Building Materials, 2011, 25(11): 4165–4174
8. Kumar B N N, Kumar P K, Babu E R, Gopal M, Reddy D S, Sreekanth K, Yellppa U. An experimental study on sea sand by partial replacement of sea sand in concrete. International Journal of Scientific Research in Science and Technology, 2016, 2(2): 181–184
9. Bravo M, de Brito J, Pontes J, Evangelista L. Mechanical performance of concrete made with aggregates from construction and demolition waste recycling plants. Journal of Cleaner Production, 2015, 99: 59–74
10. Poon C S, Kou S C, Wan H W, Etxeberria M. Properties of concrete blocks prepared with low grade recycled aggregates. Waste Management (New York, N.Y.), 2009, 29(8): 2369–2377
11. Etxeberria M, Fernandez J M, Limeira J. Secondary aggregates and

seawater employment for sustainable concrete dyke blocks production: Case study. Construction & Building Materials, 2016, 113: 586–595

12. Shi Zh, Shui Zh, Li Q, Geng H N. Combined effect of metakaolin and sea water on performance and microstructures of concrete. Construction & Building Materials, 2015, 74(15): 57–64
13. Li Q H, Geng N, Huang Y, Shui Z. Chloride resistance of concrete with metakaolin addition and seawater mixing: A comparative study. Construction & Building Materials, 2015, 101: 184–192
14. Liu J L, Mei Y, Xia R. A new wetting mechanism based upon triple contact line pinning. Langmuir, 2011, 27(1): 196–200
15. Cheng S, Shui Z, Sun T, Yu R, Zhang G Z, Ding S. Effects of fly ash, blast furnace slag and metakaolin on mechanical properties and durability of coral sand concrete. Applied Clay Science, 2017, 141: 111–117
16. Huang Y J, Wu J D, Wang Q. Behaviour of sea sand recycled concrete filled steel tube under axial compression. PICE-Structures and Buildings, 2020, 173(4): 302–312
17. Huang Y J, He X J, Sun H S, Sun Y D, Wang Q. Effects of coral, recycled and natural coarse aggregates on the mechanical properties of concrete. Construction & Building Materials, 2018, 192: 330–347
18. Da B, Yu H, Ma H, Tan Y, Mi R, Dou X. Experimental investigation of whole stress-strain curves of coral concrete. Construction & Building Materials, 2016, 122: 81–89
19. Huang Y J, Li X W, Lu Y, Wang H H, Wang Q, Sun H S, Li D Y. Effect of mix component on the mechanical properties of coral concrete under axial compression. Construction & Building Materials, 2019, 223: 736–754
20. Zuo P C, Liu J L, Li S P. The load-bearing ability of a particle raft under the transverse compression of a slender rod. Soft Matter, 2017, 13(12): 2315–2321
21. Xiao J Z, Li J B, Zhang Ch. Mechanical properties of recycled aggregate concrete under uniaxial loading. Cement and Concrete Research, 2005, 35(6): 1187–1194
22. Guo H, Shi C J, Guan X M, Zhu J P, Ding Y H, Ling T C, Zhang H B, Wang Y L. Durability of recycled aggregate concrete—A review. Cement and Concrete Composites, 2018, 89: 251–259
23. Xu J J, Zhao X Y, Yu Y, Xie T Y, Yang G S, Xue J Y. Parametric sensitivity analysis and modelling of mechanical properties of normal- and high-strength recycled aggregate concrete using grey theory multiple nonlinear regression and artificial neural networks. Construction & Building Materials, 2019, 211: 479–491
24. Etxeberria M, Vazquez E, Marí A, Barra M. Influence of amount of recycled coarse aggregates and production process on properties of recycled aggregate concrete. Cement and Concrete Research, 2007, 37(5): 735–742
25. Huang Y J, He X J, Wang Q, Xiao J Z. Deformation field and crack analyses of concrete using digital image correlation method. Frontiers of Structural and Civil Engineering, 2019, 13(5): 1183–1199
26. Choi S, Shah S P. Measurement of deformations on concrete subjected to compression using image correlation. Experimental Mechanics, 1997, 37(3): 307–313